RSC Advances

ROYAL SOCIETY
OF CHEMISTRY

www.rsc.org/advances

Tumor-targeted folate-decorated albumin stabilised silver nanoparticle induce apoptosis at low concentration in human breast cancer cells

Bharat Bhushan[1], P.Gopinath[1,2] *

Nanobiotechnology Laboratory,

Centre for Nanotechnology[1], Indian Institute of Technology Roorkee,

Department of Biotechnology[2], Indian Institute of Technology Roorkee,

Roorkee, Uttarakhand-247667, India.

*Corresponding author: Tel. +91-1332-285650; Fax. +91-1332-273560;

E-mail: pgopifnt@iitr.ernet.in, genegopi@gmail.com

Abstract

In current scenario, silver nanoparticles (Ag NPs) have been widely used in clinical and household products due to their broad spectrum antibacterial activity. But the cytotoxicity and genotoxicity associated with Ag NPs at higher concentration hindered its applications in the field of cancer therapy. The current study exploits the folate mediated delivery of bovine serum albumin (BSA) stabilized Ag NPs and thereby overcoming various drawbacks associated with non specific targeting. The albumin coating enhanced the stability of Ag NPs and also provide surface for folate conjugation *via* carbodiimide reaction. Physicochemical characterization confirms the formation of folate-decorated albumin stabilized Ag NPs (FA-BSA-Ag NPs). The prepared nanoparticles depict admirable binding, especially in case of MCF-7 (FR-positive cells) having abundant folate receptor (FR) on its surface that leads to their enhanced cellular internalization as compared to A549 cells (FR negative cells). The cell viability assay corroborates a better therapeutic efficacy of prepared NPs against MCF-7 cells as compared to A549 cells. The flow cytometer analysis reveals reactive oxygen species (ROS) increment that leads to oxidative stress induced apoptosis in both the cells. Further cell cycle, morphological and nuclear analysis suggests characteristic apoptosis indications, which was further confirmed by gene expression analysis. Altogether, these studies implied that the tumor-targeted FA-BSA-Ag NPs induce apoptosis in MCF-7 cells at much lower Ag NPs concentration. In future, these targeted albumin stabilized Ag NPs could provide a more safe and effective alternative approach in the field of cancer therapy.

KEYWORDS

2

Introduction

In recent years, metal and semiconductor nanoparticles found tremendous applications in the field of nanomedicine [1-3]. The triumph of food and drug administration (FDA) approved Acticoat (Ag NPs based wound dressing bandage) develop tremendous interest among the scientific community [4]. Since then silver nanoparticles have been extensively studied either alone or in composites form for their antibacterial and anticancer potential [5-8]. Moreover, our previous studies corroborates that apart from disturbing the membrane integrity and normal function of the cells, Ag NPs by themselves or in combination with other therapeutic agents successfully induce apoptosis in various human cancer cells [2]. The therapeutic potential of Ag NPs lies in their ability to augment the ROS generation and activate mitochondria dependent apoptosis [9]. However, major drawbacks associated with Ag NPs such as genotoxicity and DNA damaging capability hindered their therapeutic applications [10-11]. This provokes a need to develop a safe and effective system for efficient delivery of Ag NPs with enhanced therapeutic efficacy at lowest possible Ag NPs concentrations and thereby provide an alternative mode of cancer therapy.

In this regard, protein based nanoparticles have been emerged as a potential candidate for therapeutic applications because of their high biocompatibility, high water solubility, biodegradability, good availability, easy surface modification, non-toxic and non-immunogenic properties [1, 12-13]. With the success of FDA approved Abraxane (albumin based drug nano-formulation), albumin based nanoparticles emerged as a potential candidate in the field of nanotechnology and cancer therapy [14-17]. Moreover, the presence of functionally charged groups including amino and carboxylic groups offer albumin with various possibilities for surface modification and interaction with various nanoparticles and

drug molecules [13]. The biocompatible albumin coating around the NPs enhanced their stability and consequently provide surface for the attachment of various functional targeting moieties.

The current conventional therapies have many unresolved challenges including non-specific accumulation of the therapeutic molecules, which results in reduced therapeutic efficacy, enhanced toxicity of neighbour tissues and limits the maximum dose availability [18]. These drawbacks need to be addressed in order to develop an efficient tumor-targeted therapeutic system for cancer therapy. Until now, researchers have exploited the natural endocytosis pathways for the efficient delivery of therapeutic agents into the cells [19]. A vast variety of cancer specific ligands have been explored so far for the enhanced delivery and retention of therapeutic molecules inside the tumor tissue [20]. Among them folate and their conjugates shows tremendous affinity towards the folate binding protein i.e. FR, which became a confirmed target for non-destructive cancer specific delivery of therapeutic molecules [21, 22]. Folic acid (FA), a natural ligand for FR is a vital dietary vitamin required for the DNA biosynthesis, cell proliferation and metabolism [20]. The FR is present specifically in abundance on the surface of variety of cancer cells including ovary, breast, kidney, myeloid and brain cells as compared to normal tissues [23, 24]. Moreover, the high binding affinity towards FR, small size, non-immunogenic, high stability, ease of attachment, low cost, high availability and high tumor specificity make it an ideal candidate for targeted cancer imaging and therapy [25-29]. To date a large number of folate conjugated albumin based nanoparticles have been successfully synthesized for various targeted cancer diagnosis and therapeutic approaches as illustrated in Table S1 [26-36]. Apart from targeted delivery of anticancer drugs and imaging agents, a variety of folate conjugated albumin stabilized inorganic nanoparticles have been extensively utilized due to its unique properties. Among them, gold

based nanostructures have been widely used in targeted cancer imaging and photo thermal therapy (PTT), while iron oxide based nanoparticles found their extensive utilization in magnetic resonance imaging (MRI) and hyperthermia [26-28, 32, 33]. In this paper, the anticancer potential of Ag NPs has been explored by preparing FR targeted FA-BSA-Ag NPs with enhanced therapeutic efficacy, improved bioavailability, and efficient aqueous solubility by carbodiimide covalent reaction. Such system is further characterized and evaluated for their role in successful induction of apoptosis in human breast and lung cancer cells *in vitro*. The results corroborates that the FA-BSA-Ag NPs successfully induce apoptosis even at lower Ag NPs concentration as a result of improved bioavailability.

Experimental section

Materials

BSA and dimethyl sulfoxide (DMSO) was obtained from HIMEDIA. Silver nitrate (AgNO$_3$) and sodium borohydride (NaBH$_4$) were procured from Merck (Germany). The cross-linking agent glutaraldehyde (50 wt% in H$_2$O), propidium iodide (PI), 1-ethyl-3-(3-dimethylaminopropyl)-carbodiimide hydrochloride (EDC) and N-hydroxy succinimide (NHS) and 2',7'- dichlorfluorescein diacetate (DCFH-DA) were procured from Sigma–Aldrich. The cell staining dyes rhodamine B (Rho B) and Hoechst 33342 were purchased from life technologies. All other chemicals used were molecular biology grade. MCF-7 (Breast cancer cells) and A549 cells (Non-small lung cancer cells) were received from National Centre for Cell Science, Pune, India and maintained in Dulbecco's modified Eagle's

medium (DMEM) containing 10% calf serum and 1% Penicillin-streptomycin in the humidified incubator with 5% CO_2 at 37°C.

Preparation of FA-BSA-Ag NPs

Albumin stabilized Ag NPs was synthesized using $NaBH_4$ reduction method as reported earlier [37, 38]. Briefly, BSA (25mg mL^{-1}) was dissolved in 10 mL of deionized water and then $AgNO_3$ (50 mM) was added into the above solution at 25°C under vigorous stirring. The pH of the solution was maintained at pH =8 with 0.1 M NaOH. After 5 min, silver ions were reduced by drop-wise addition of $NaBH_4$ (10 mM), until the colour of solution changes from colourless to brown colour. The solution was stirred overnight in dark. The BSA-Ag NPs were conjugated with FA according to the standard procedure reported earlier [29-32, 34]. An active ester intermediate (NHS–folate) was prepared by the reaction of EDC/ NHS with the carboxyl groups of FA, which in turn covalently conjugated with the amine groups of BSA. Briefly, FA (27 mg) was dissolved in 2 mL DMSO, followed by addition of EDC (58.6 mg) and NHS (35.2 mg) and allowed to stir in dark for 3 h. Consequently, the pre-activated FA mixture was slowly added to the BSA-Ag NPs solution under alkaline condition (pH adjusted to 10 by 1M NaOH). The solution was allowed to stir overnight in dark at room temperature. The solution was then continuously dialyzed for 3 days and further purified by using Sephadex G-25 column to remove excess FA and other reactants. The final solution obtained was filtered and stored in amber color bottle at 4°C, until further used.

Characterizations

6

UV-visible spectroscopic measurement was done on Lasany double beam L1 2800 UV-visible spectrometer. Fourier transform infrared spectroscopy (FTIR) spectra were recorded on Thermo Nicolet FTIR spectrometer using KBr pellets in the range of 4000-400 cm^{-1}. The particle size, morphological and elemental mapping were performed using field emission scanning electron microscope (FE-SEM, Carl Zeiss ULTRA PLUS) having energy dispersive X-ray (EDX) detector and transmission electron microscope (TEM, TECNAI G^2 20 S-TWIN) operating at 200 kV. A size distribution histogram of prepared Ag NPs was analysed using ImageJ (http://rsb.info.nih.gov/ij/download.html). X-ray diffraction (XRD) analysis was carried out by using Bruker AXS D8 advance powder X-ray diffractometer (Cu-Kα radiation, λ = 1.5406A˚) in the range of $10–90^{o}$ at a scan speed of 0.5^{o}/min. Thermal analysis was conducted on EXSTAR TG/DTA 6300 at a constant rate of $10^{o}C$/ min under controlled nitrogen atmosphere, while concentration of Ag NPs were analyzed by inductively coupled plasma mass spectroscopy (ICP-MS, Perkin-Elmer ELAN DRC-e).

Cell viability assay

The cytotoxicity of as-prepared FA-BSA-Ag NPs was evaluated on MCF-7 and A549 cells *via* 3-(4, 5-dimethylthiazol-2-yl)-2,5-diphenyltetrazolium bromide (MTT) assay or cell viability assay. The MTT is mitochondrial based assay depend on the ability of viable cell to convert the tetrazolium salt to purple color formazan crystals. Briefly, 10^{4} cells were seeded in a 96 well plate (Corning, Costar, NY). After overnight attachment cells were treated with different concentrations of BSA, BSA-Ag NPs and FA-BSA-Ag NPs for 24 h. Following incubation, the spent medium was removed and cells were given phosphate buffered saline (PBS) wash and then incubated with fresh 100 μL DMEM medium containing 10 μL of MTT dye (5 mg mL^{-1}) for 3-4 h at $37^{o}C$. Finally the supernatant medium was aspirated and

7

formazan crystals formed were dissolved by adding 100 μL of lysis solution and incubate over gyratory shaker at room temperature for 30 min. The absorbance of the finally dissolved product was taken at 570 nm and 690 nm by using a multimode reader (Cytation 3, Biotek).

Acridine orange/ethidium bromide (AO/EB) dual staining

In order to differentiate apoptotic nuclei from necrotic nuclei, the FA-BSA-Ag NPs treated A549 and MCF-7 cells were stained with AO/EB dual dye [17]. Briefly, 2×10^5 cells per well were seeded in a 6 well plate and allow to adhere. After overnight attachment, cells were treated with desired concentrations of FA-BSA-Ag NPs for 24 h. The treated cells were then given a PBS wash followed by incubation with AO/EB (10 μg mL^{-1} working concentration) for 5-10 min at 37 °C. Subsequently, the spent medium was removed and PBS wash was given to remove excess dyes before visualizing the cells and images were captured under different filters using cell imaging system (EVOS FL, Life Technologies, USA)

Cell morphology analysis by FE-SEM

For cell morphological analysis, A549 and MCF-7 cells were seeded on a sterile glass cover slip and incubated overnight for attachment. The cells were then treated with desired concentrations of FA-BSA-Ag NPs for 24 h and then fixed by using 2% glutaraldehyde for 10 min followed by ethanol gradient fixation. The fixed cells were then air dried and sputter coated with gold before examined under FE-SEM.

Time dependent morphological examination

The events of apoptosis such as nuclear chromatin compaction and cytoskeleton alteration were examined *via* Hoechst 33342 and rhodamine B (Hoechst-rho B) fluorescent dual dyes combinations. Briefly, 2×10^5 cells per well were seeded in a 6 well plate and after attachment, cells were treated with FA-BSA-Ag NPs for different time periods. After treatment spent media were removed and cells were given a brief PBS wash, followed by incubation with 2 μL Hoechst dye (stock concentration-10 mg mL^{-1}) and 5 μL Rho B (stock concentration- 1 mg mL^{-1}) at 37 °C for 10–15 min. Thereafter, overlay images were obtained under red and DAPI filters.

In vitro cellular uptake studies

A quantitative analysis of Ag uptake by the A549 and MCF-7 cells was done by using ICP-MS analysis. Briefly, 2×10^5 cells were seeded in 3.5 cm cell culture plate and after overnight attachment; cells were treated with desired concentrations of FA-BSA-Ag NPs for 3 h. In order to remove all extra cellular FA-BSA-Ag NPs, the treated cells were given extensive PBS wash and then harvested and counted. The cells were finally acid digested by using concentrated nitric acid for 24 h. The digested sample was then diluted with deionized water and Ag concentration was determined by ICP-MS.

Intracellular ROS generation

A549 and MCF-7 cells were seeded in a 6 well plate and incubated overnight for attachment followed by treatment with desired concentration of FA-BSA-Ag NPs for 3h. After treatment cells were given brief PBS wash followed by incubation with medium supplemented with 20

µM DCFH-DA dye for 20 min at 37 °C. The cells were then harvested and analyzed immediately by using flow cytometer (Amnis Flowsight). The DCFH-DA is a membrane permeable dye used to measure intracellular ROS activity. Inside the cells the DCFH-DA is cleaved by intracellular esterases and finally converted into highly fluorescent 2,7-dichlorofluorescein (DCF) in presence of ROS [3]. The fluorescence intensity of DCF is detected in channel 2 (Intensity_MC_02). The data were acquired for 10,000 cells per sample and acquired data were analyzed through Amnis Ideas software.

Cell Cycle Analysis

The effect of FA-BSA-Ag NPs on the cell cycle of A549 and MCF-7 cells was determined by PI staining and consequent analysis by flow cytometry as described earlier [39]. Briefly, 2x 10^5 cells were seeded in a 6-wells plate and incubated overnight at 37°C for attachment. The cells were then treated with desired concentration of FA-BSA-Ag NPs for 24 h. The cells were carefully harvested by trypsinization to prevent the loss of floating cells, followed by fixation with 70% alcohol for 15 min on ice. The fixed cells pellet obtained after centrifugation were then incubated with PI staining solution (50 µg/mL PI, 1 mg/mL RNase A, and 0.05% triton X-100) for 30 min at 37° C in dark. The PI stained cells were then analysed through flow cytometer to determine the cell cycle distribution. A total of 10,000 events per sample were captured and analyzed through IDEAS software.

Gene expression studies

For gene expression analysis, cells were grown in a 6 well plate followed by treatment with appropriate concentration of FA-BSA-Ag NPs for 24 h. Thereafter, total RNA was isolated from the cells by using Tri reagent (Sigma Aldrich, USA) and cDNA were synthesized by using Superscript II Reverse Transcriptase (Invitrogen, USA) from 1 μg of denatured RNA at 42 ^{o}C for 50 min. Differential expression of apoptotic signalling genes were analyzed by using semi-quantitative reverse transcriptase-polymerase chain reaction (RT-PCR) analysis by taking house- keeping gene β-actin as internal control. Briefly, 1μL of above RT product was taken with gene specific primers as mention in Table S4. The PCR cycle was carried out in Veriti 96 well thermal cycler (Applied Biosystems) at 94 °C for 3 min (initial denaturation), followed by a PCR cycle at 94 °C for 30 s (denaturation), at 60 °C for 30 s (annealing), at 72 °C for 1 min (extension) and at 72 °C for 10 min (final extension). The final amplified PCR products were visualized and resolved on 1.2% agarose gel containing ethidium bromide under UV light. The band intensity was quantified by using Image lab 4.0 software.

Results and discussion

Synthesis and characterization of FA-BSA-Ag NPs

The objective of current study is to develop an albumin based targeted therapeutic agent, where it serves the dual purpose by acting as a stabilizer of Ag NPs and provide free amino groups for the attachment of targeting moieties such as folic acid as shown in Fig. 1. The Ag NPs were synthesized by NaBH$_4$ reduction method in the presence of albumin. The formation of albumin stabilized Ag NPs was primarily studied by UV-visible spectroscopy showing the

appearance of typical plasmonic band at 420 nm as shown in Fig. S1. In the next step, folic

acid a tumor-targeting moiety was conjugated to the amines groups present on the surface of

BSA-Ag NPs *via* EDC/NHS coupling chemistry. The EDC and NHS activate the carboxylic

acid groups of the folic acid which in turn combined with the amine groups of albumin. Fig.

S2 and S3 correspond to the elemental distribution and EDS pattern of FA-BSA-Ag NPs

showing the existence of silver in the complex. The size and shape of the prepared NPs was

determined by using TEM as shown in Fig. 2 (a). TEM image depicts that particles are

spherical in shape having an average size around 8.21±2.98 nm; the size distribution

histogram of FA-BSA-Ag NPs is shown in Fig. 2 (b). The bright spots in the selected area

electron diffraction (SAED) pattern attributed to the crystalline nature of the Ag NPs with

phases (111), (200), (220) and (311).

Figure 3 (b) represent the XRD pattern of FA-BSA-Ag NPs. A well defined characteristic

diffraction peak appeared at 38.07° that corresponds to (111) crystal plane of elemental silver

depicting the presence of Ag NPs [37]. In addition, broader peaks appeared around 20 $^{\circ}$ as a

result of amorphous nature of the coated albumin layer. Moreover, the thermo gravimetric

(TG) analysis of BSA-Ag NPs, FA-BSA-Ag NPs and BSA alone were carried out under

nitrogen atmosphere illustrating the slower rate of degradation for albumin- Ag NPs

complexes i.e. BSA-Ag NPs and FA-BSA-Ag NPs as compared to pristine BSA. From Fig. 3

(a), it is clearly evident that the degradation of particles start from 200 $^{\circ}$C and beyond 250 $^{\circ}$C,

a sudden weight loss was observed which account to the loss of small molecules i.e.

ammonia, CO_2 etc. Around 400–500 $^{\circ}$C, a substantial difference in weight loss was

examined, as 21% was left for pristine BSA, 38% was left for FA-BSA–Ag NPs and 40%

was remaining for BSA-Ag NPs indicating the improved stability of BSA–Ag NPs and FA-

BSA-Ag NPs as compared to pristine BSA. Beyond 500 $^{\circ}$C, a rapid rate of degradation was

noticed in case of BSA-Ag NPs, which may be as a result of crystalline nature of Ag NPs. However, a slower rate of degradation was observed for FA-BSA-Ag NPs due to the presence of folic acid. Moreover, beyond 600 $^{\circ}$C no significant change was noticed for BSA and BSA-Ag NPs due to the char formation, while in case of FA-BSA-Ag NPs a sudden weight loss was found, thus confirming the presence of folic acid [37].

The conjugation of BSA-Ag NPs with FA is typified by FTIR analysis. The FTIR spectrum of FA, BSA-Ag NPs and FA conjugated BSA-Ag NPs are shown in Fig. 4. The characteristic peaks of BSA-Ag NPs and FA alone were illustrated in Table S2 and S3 [3, 40]. On comparing the BSA-Ag NPs with FA-BSA-Ag NPs, a major shift in the peaks were observed from 3306.5 to 3331.1, 2959.57 to 2931.51, 1537.43 to 1540.39, 1391.6 to 1397.52, 1242.2 to 1247.69 cm^{-1} corresponding to the stretching vibration of –OH groups, stretching vibration of N-H groups, stretching vibration of C-O groups and N-H bend respectively, along with other peaks shift confirms the interaction between the FA and BSA-Ag NPs. In case of FTIR spectrum of the FA-BSA–Ag NPs, a peak was observed at 1021.06 cm^{-1} as a result of augmented –CH bending of alkenes and a decline in anhydride C–O stretching of FA involved in the reaction.   Moreover, the appearance of new peaks at 1451.39 cm^{-1}, corresponding to the phenyl ring of folic acid along with other bands confirms the successful conjugation of FA to the BSA-Ag NPs [41, 42].

In vitro cytotoxicity

In vitro cytotoxicity assay of BSA-Ag NPs and FA-BSA-Ag NPs was assessed *via* MTT assay on MCF-7 and A549 cells. An up-regulation of FR is observed in specific cancer cells such as human breast cancer cells, MCF-7. Thus the FA-BSA-Ag NPs specifically target the

MCF-7 (FR-positive cells) as compared to A549 (FR-negative cancer cells). In Fig. S4 the

bare BSA was analyzed for their cytotoxicity against both the cells and found to be non-toxic.

After 24 h, more than 90 % cell viability was found which shows the biocompatibility of

BSA. Thus the results suggest that the therapeutic efficacy of FA-BSA-Ag NPs is due to Ag

NPs and not because of the stabilizing agents.

Moreover, the effect of BSA-Ag NPs and FA-BSA-Ag NPs on the viability of A549 and

MCF-7 cells were evaluated by MTT assay as illustrated in Fig.5, the results suggests a

concentration dependent inhibition of cell viability by BSA-Ag NPs and FA-BSA-Ag NPs.

However, the cell inhibition capability of FA-BSA-Ag NPs was enhanced significantly

(around 2.59 fold) in MCF-7 as compared to BSA-Ag NPs, while a little increment was

observed (around 1.36 fold) for A549 cells. The IC_{50} value of BSA-Ag NPs was found to be

14.21 and 5.97 μg mL $^{-1}$ and of FA-BSA-Ag NPs was found to be 11 and 2.3 μg mL $^{-1}$ on

A549 and MCF-7 cells respectively, illustrating that the FA-BSA-Ag NPs exhibit excellent

cytotoxicity against both the cells as compared to BSA-Ag NPs. However, the enhanced

antitumor efficacy and greater suppression effect was observed on MCF-7 (FR-positive cells)

treated with FA-BSA-Ag NPs. Thus the results suggests that the FA modification of BSA-Ag

NPs improve therapeutic efficacy by facilitating the FR mediated cellular uptake and

therefore induce apoptosis at much lower concentration of Ag NPs.

AO/EB dual staining

14

The mode of cell death in FA-BSA-Ag NPs treated A549 and MCF-7 cells was determined by staining the cells with a combination of fluorescent DNA intercalating dual dyes (i.e. AO/EB) and then examined them under fluorescent microscope. The AO dye is taken up by both viable and non viable cells and gives green fluorescence after binding with double stranded DNA. While, EB can permeate only membrane compromised cells and bind to the double stranded DNA to produce red fluorescence. The difference in the permeation capability of both dyes makes it possible to differentiate between the viable, apoptotic and necrotic cells [43]. The viable healthy cells effectively exclude the EB stain and it appears uniform green colored fluorescent nucleus due to the presence of AO alone as shown in Fig.6 (a and e). Similarly, the cells treated with half the IC_{50} concentration does not show any significant change in the cells morphology and also emit green color fluorescence as shown in Fig. 6 (b and d). While the cells treated with IC_{50} and 2 x IC_{50} concentrations shows typical morphological changes corresponds to the apoptosis such as cytoplasmic constriction, membrane blebbing and nuclear fragmentation [43, 44]. Fig. 6 (c-d and g-h), clearly demonstrate the existence of early apoptosis (EA) characterized by condensed chromatin in the treated cells along with late apoptosis (LA) characterized by fragmented nuclei and apoptotic bodies. These morphological changes clearly depict the induction of apoptosis in the A549 and MCF-7 cells treated with FA-BSA-Ag NPs. Moreover, the FA modification augmented the apoptosis effect in MCF-7 cells as compared to A549, which may be due to the different expression levels of FR on the surface of two cells. The MCF-7 cells actively adsorbed FA-BSA-Ag NPs *via* folic acid mediated endocytic pathway. Thus, the above results are in correlation with the results obtained from MTT assay.

FE-SEM studies

Further morphological assessment of induction of apoptosis was done in FA-BSA-Ag NPs treated A549 and MCF-7 cells by using FE-SEM analysis. Fig. 7 (a and c) clearly depict the characteristic healthy morphology of untreated cells which adhere well to the surface with no substantiation of membrane constriction. While, in case of cells treated with FA-BSA-Ag NPs shows loosely attached rounded spherical morphology as compared to untreated cells as shown in Fig.7 (b and d). Moreover, the events of apoptotic cell death such as membrane blebbing, formation of apoptotic bodies and cytoplasmic constriction were clearly visible in both the cell lines [44].

Hoechst-rho B staining

In addition to AO-EB and FE-SEM analysis, further time dependent assessment of induction of apoptosis was done by using Hoechst-rho B staining to monitor the cytoskeleton compaction and nuclear fragmentation. Hoechst 33342, a membrane permeable dye that stain nucleus and emit blue fluorescence on combining with the dsDNA. It is used to differentiate the untreated cells having normal nucleus with apoptotic cells having nucleus with condensed chromatin (pycnotic nucleus) [45]. On the other hand rho B stains the cytoplasm and mitochondria of the cells [43]. Fig. 8 and Fig. S5 clearly depict the time dependent chromatin condensation in the nucleus appearing in the form of dark spots (indicated by white arrows) accompanied with simultaneous cytoplasm constriction (as indicated by yellow arrows). Moreover, after 24 h of incubation a significant number of pycnotic nuclei were observed suggesting apoptotic mode of cell death. Altogether, all these morphological analysis suggest the role of FA-BSA-Ag NPs in inducing apoptotic cell death in A549 and MCF-7 cells.

Cellular uptake study

As reported earlier, the FA conjugates bind to the FR on the cancer cells with same affinity as that of FA alone and get internalized through plasma membrane *via* FA mediated specialized endocytosis and vesicular trafficking [46]. In order to quantify the uptake of silver nanoparticles by MCF-7 and A549 cells, ICP-MS analysis were conducted. Both the cells were treated with different concentration of FA-BSA-Ag NPs for 3h. As shown in Fig. 9, a concentration dependent increase in the Ag NPs uptake was observed for both cells. However, amount of Ag NPs uptake was found to be significantly higher in case of MCF-7 as compared to A549 cells suggesting the successful FA mediated targeted delivery of Ag NPs in MCF-7 cells. This held accountable for the higher cytotoxicity in MCF-7 as compared to A549 as observed in MTT assay.

Intracellular ROS determination

ROS induced oxidative stress is one of the crucial factors responsible for the cytotoxicity of Ag NPs as reported earlier [47, 48]. Intrinsic antioxidant defence system protects the body against ROS by keeping a balance between the oxidant/antioxidant levels in the cells. However, excessive ROS generation caused due to the impaired antioxidant defence system of the body lead to the induction of oxidative stress, which finally results in the DNA damage, mitochondrial dysfunction and apoptotic cell death [3, 39]. The ROS levels on FA-BSA-Ag NPs treatment was investigated by using DCFH-DA assay using flow cytometer in order to assess their potential role in oxidative stress mediated cell death. Fig. 10 depicts the level of ROS generation in FA-BSA-Ag NPs treated MCF-7 and A549 cells. The percentage of ROS producing cells were 2% and 2.4% in untreated MCF-7 and A549 cells respectively, which increased to 8.4% and 5 % on treating the MCF-7 and A549 cells respectively with $0.5x$ IC_{50} concentration. Moreover, in case of cells treated with IC_{50} and $2 \times IC_{50}$

concentrations a significant increase in the ROS level was found. In MCF-7 the elevated ROS level at IC_{50} and 2x IC_{50} concentrations was found to be 24.1 and 41.2 % as compared to 18.1 and 26.3 % of ROS producing cell population in A549 cells respectively. These results suggest that the FA-BSA-Ag NPs induced more oxidative stress in MCF-7 as compared to A549 cells due to the FA mediated targeted delivery of Ag NPs that evokes more ROS generation in MCF-7 cells. The results are in correlation with the MTT and uptake studies.

Cell Cycle Analysis

Ag NPs is well known to induce oxidative DNA damage and chromosomal aberrations that results in the cell cycle arrest [10, 39]. The induction of apoptotic mode of cell death on FA-BSA-Ag NPs exposure was measured by PI staining, followed by flow cytometric analysis. Fig. 11 demonstrate the effect of FA-BSA-Ag NPs on the cell cycle distribution pattern of A549 and MCF7 cells incubated with desired concentrations FA-BSA-Ag NPs for 24 h. The results depicted that low concentration of FA-BSA-Ag NPs (i.e. 0.5x IC_{50}) did not produce any notable change in the cell cycle as compared to the untreated cells; most of the cells were found to be primarily arrested in G0/G1 phase. However, at higher concentration (i.e. IC_{50} and 2x IC_{50}), a noticeable increase in the sub G0/G1 population accompanied by decrease in G0/G1 phase was observed with respect to untreated cells. Moreover, a marked decrease in the S phase was also monitored upon FA-BSA-Ag NPs exposure. Thus, an increase in the sub G0/G1 phase and decrease in the S phase population at IC_{50} and 2x IC_{50} corresponds to the apoptotic mode of cell death [49, 50].

Gene expression analysis

The potential of FA-BSA-Ag NPs to provoke apoptosis in human lung and breast cancer cells were investigated *in vitro* by means of semi-quantitative RT-PCR analysis, results suggested that the involvement of various pro-apoptotic signalling genes includes caspase 3, bax, bad, c- myc, p53 and anti-apoptotic signalling genes including bcl-xl as shown in Fig. 12. While, β-actin (housekeeping gene) was taken as internal control, whose expression remains unaltered during the process. As depicted in Fig.12 (a) an up-regulation was observed in the expression of pro-apoptotic genes (indicated by upward arrow), while the expression of anti-apoptotic genes was found to be down-regulated (indicated by downward arrow). Moreover, the fold change in the expression of genes was shown in Fig. 12 (b).

The apoptotic pathway involved in the FA-BSA-Ag NPs treated cells was shown in Fig. 12 (c). The FA-BSA-Ag NPs treatment leads to membrane destabilization and intracellular ROS generation, which in turn activates the intracellular signalling pathway that finally results in the activation of p53 [5,6]. The anti-apoptotic bcl-xl (basal cell lymphoma-extra large), a member of bcl-2 family located on the outer mitochondrial membrane prevent the cells from entering into apoptotic pathway by blocking the mitochondrial release of cytochrome-c by controlling the membrane permeability either via formation of pores or by creating an ion channel [51]. While pro-apoptotic bax (bcl-2-associated X protein) and bad (bcl-2-associated death promoter) promote such release and thereby endorses apoptosis by inhibiting the anti-apoptotic function of bcl-xl [52, 53]. A down-regulation in the expression of bcl-xl along with subsequent up-regulation of bad and bax suggests a successful initiation of apoptosis. Moreover, as reported earlier p53 is found to be involved in the up-regulation of bax [54]. An increase in the expression of bax suggests the involvement of p53 in the apoptotic cell death in FA-BSA-Ag NPs treated cells. Further, outer membrane permeabilization (MOMP) results in the translocation of bax from cytosol to mitochondria, which leads to the release of

cytochrome c, a pro-apoptotic molecule into the cytoplasm *via* pores formation [54]. Finally, the cytochrome c activate the caspase-3 (cysteine-aspartic acid proteases), a key factor both in the initiation and execution of apoptosis and also accountable for the cellular DNA fragmentation during apoptosis [55-57]. An up-regulation in the expression of caspase-3 suggests their role in the apoptosis in FA-BSA-Ag NPs treated cells. In addition to that an increased expression of C-myc, a well known inducer of apoptosis was also observed, which further validate the p53 mediated apoptotic cell death. Our results were found in correlation with the previous studies [5, 9]. Thus the above mentioned gene expression profiles clearly demonstrated the p53 mediated apoptotic cell death along with consequent cell blebbing in the FA-BSA-Ag NPs treated A549 and MCF-7cells.

Conclusions

In the present study, folate-decorated albumin stabilized Ag NPs are synthesized. The albumin coating not only provides stability but also provide charged amino groups required for the folic acid conjugation. The physicochemical characterization demonstrates the successful folate modification of NPs necessary for their targeted delivery. The MTT assays revealed the higher therapeutic efficacy of folate modified NPs as compared to unmodified NPs against FR positive human breast cancer cells. The cellular uptake study reveals enhanced uptake in MCF-7 as compared to A549 cells due to the cancer specific targeting of Ag NPs. Moreover, the morphological and nuclear analysis suggests successful initiation of apoptosis in both the cancer cells. Further, flow cytometer and gene expression analysis corroborates the efficient induction of apoptosis by two separate mechanistic ways including: ROS production and induction of apoptotic signalling pathway in both the cancer cells. Thus, the current studies proposed that the folate modified albumin stabilized Ag NPs elicit anti-

proliferative response and induce apoptosis in FR positive cells at much lower concentration and thereby reduce the complications that hinders their role in the future nanomedicine and cancer therapeutic applications.

References

1. U. K. Sukumar, B. Bhushan, P. Dubey, I. Matai, A. Sachdev and P. Gopinath, *Int. Nano Lett.*, 2013, **3**, 45–53.

2. P. Gopinath, S. K. Gogoi, A. Chattopadhyay and S. S. Ghosh, *Nanotechnology*, 2008, **19**, 075104.

3. B. Bhushan and P. Gopinath, *J. Mater. Chem. B*, 2015, **3**, 4843-4852.

4. V. C. Mazurak, R. E. Burrell, E. E. Tredget, M. T. Clandinin and C. Field, *J. Burns.*, 2007, **33**, 52.

5. P. Gopinath, S. K. Gogoi, P. Sanpui, A. Paul, A. Chattopadhyay and S. S. Ghosh, *Colloids Surf., B*, 2010, **77**, 240–245.

6. P. Dubey, I. Matai, S. U. Kumar, A. Sachdev, B. Bhushan and P. Gopinath, *Adv. Colloids Inter. Sci., B*, 2015, **221**, 4-21.

7. P. Dubey, B. Bhushan, A. Sachdev, I. Matai, S. U. Kumar and P. Gopinath, *J. App. Polm. Sci.*, 2015, **42473**, 1-12.

8. I. Matai, A. Sachdev, P. Dubey, S. U. Kumar, B. Bhushan and P. Gopinath, *Colloids Surf., B*, 2014, **115**, 359–367.

9. Y.H. Hsin, C. F. Chen, S. Huang, T. S. Shih, P. S. Lai, P. Chueh, *J. Toxicol. Lett.* 2008, **179**, 130-139.

10. P. V. Asharani, G. L. K. Mun, M. P. Hande, S. Valiyaveettil, *ACS Nano* 2009, **3**, 279.

11. P. V. Asharani, Y. L. Wu, Z. Gong, S. Valiyaveettil, *Nanotechnology*, 2008, **19**, 255102.

12. B. Bhushan, U. K. Sukumar, I. Matai, A. Sachdev, P. Dubey and P. Gopinath, *J. Biomed. Nanotechnol.*, 2014, **10**, 2950–2976.

13. P. Gopinath, S. Uday Kumar, I. Matai, B. Bhushan, D. Malwal, A. Sachdev and P. Dubey, Cancer Nanotheranostics., *Springer briefs in applied science and technology* ., 2015, 1-93.

14. N. K. Ibrahim, N. Desai, S. Legha, P. Soon-Shiong, R. L. Theriault, E. Rivera, B. Esmaeli, S. E. Ring, A. Bedikian, G. N. Hortobagyi and J. A. Ellerhorst, *Clin. Cancer Res.*, 2002, **8**, 1038–1044.

15. E. Miele, G. P. Spinelli, E. Miele, F. Tomao and S. Tomao, *Int. J. Nanomed.*, 2009, **4**, 99–105.

16. M. R. Green, G. M. Manikhas, S. Orlov, B. Afanasyev and A. M. Makhson, *Ann. Oncol.*, 2006, **17**, 1263–1268.

17. B. Bhushan, P. Dubey, S. Uday Kumar, A. Sachdev, I. Matai and P. Gopinath, *RSC Adv.*, 2015, **5**, 2078–12086.

18. F. H. Wang, D. R. Zhang, C. X. Duan, L. J. Jia, F. F. Feng, Y. Liu, Y. C. Wang, L. L. Hao and Q. Zhang, *Carbohydr. Polym.*, 2011, **84**, 1192–1200.

19. A. Gabizon, A. T. Horowitz, D. Goren, D. Tzemach, F. Mandelbaum-Shavit, M. M. Qazen and S. Zalipsky, *Bioconjugate Chem.*, 1999, **10**, 289–298.

20. Y. J. Lu and P. S. Low, *Adv. Drug Delivery Rev.*, 2002, **54**, 675– 693.

21. C. P. Leamon and P. S. Low, *Proc. Natl. Acad. Sci. U. S. A.*, 1991, **88**, 5572–5576.

22. J. Sudimack and R. J. Lee, *Adv. Drug Delivery Rev.*, 2000, **41**, 147–162.

23. R. J. Lee and P. S. Low, *Biochim. Biophys. Acta*, 1995, **1233**, 134–144.

24. C. M. Paulos, M. J. Turk, G. J. Breur and P. S. Low, *Adv. Drug Delivery Rev.*, 2004, **56**, 1205–1217.

25. C. P. Leamon and J. A. Reddy, *Adv. Drug Delivery Rev.*, 2004, **56**, 1127–1141.

26. H. Chen, S. Li, B. Li, X. Ren, D. M. Mahounga, S. Cui, Y. Gu and S. Achilefu, *Nanoscale*, 2012, **4**, 6050–6064.

27. M. Z. Fahmi, K. L. Ou, J. K. Chen, M. H. Ho, S. H. Tzing and J. Y. Chang, *Rsc Adv.*, 2014, **4**, 32762–32772.

28. H. Hao, Q. Ma, F. He and P. Yao, *J. Mater. Chem. B*, 2014, **2**, 7978–7987.

29. H. Meng, J. Y. Chen, L. Mi, P. N. Wang, M. Y. Ge, Y. Yue and N. Dai, *JBIC, J. Biol. Inorg. Chem.*, 2011, **16**, 117–123.

30. C. Du, D. Deng, L. Shan, S. Wan, J. Cao, J. Tian, S. Achilefu and Y. Gu, *Biomaterials*, 2013, **34**, 3087–3097.

31. J. Li, R. Cai, N. Kawazoe and G. Chen, *J. Mater. Chem. B*, 2015, **3**, 5806–5814.

32. R. Yang, Y. An, F. Miao, M. Li, P. Liu and Q. Tang, *Int. J. Nanomedicine*. 2014, **4**, 4231-4243.

33. Q. F. Lin, S. F. Leung, K. H. Tsui, B. Hua and Z. Y. Fan, *Nanoscale Res. Lett.*, 2013, **8**, 170.

34. L. Qi, Y. Guo, J. Luan, D. Zhang, Z. Zhao and Y. Luan, *J. Mater. Chem. B*, 2014, **2**, 8361–8371.

35. C. Su, H. Li, Y. Shi, G. Wang, Liwei Liu, L. Zhao and R. Su, *Int. J. Pharm.*, 2014, **474**, 202–211.

36. A. Martinez, E. Muniz, C. Teijon, I. Iglesias, J.M. Teijon and M.D. Blanco, *Pharm. Res.*, 2014, **31**, 1264–1274.

37. A. Gebregeorgis, C. Bhan, O. Wilson and D. Raghavan, *J. Colloid Interface Sci.*, 2013, **389**, 31–41.

38. D. Zhang and H. Yang, *Appl. Phys. A.*, 2013, **112**, 739-745.

39. S. Sharma, S. Chockalingam, P. Sanpui, A. Chattopadhyay and S. S. Ghosh, *Adv. Healthc Mater.*, 2014, **3**, 106.

40. M. G. El-Wahed, M. S. Refat and S.M. El-Megharbel, *Spectrochimica. Acta Part A*, 2008, **70**, 916–922.

41. A. Ray Chowdhuri, S. Tripathy, C. Haldar, S. Chandra, B. Das, S. Roy and S. K. Sahu, *RSC Adv.*, 2015, **5**, 21515–21524.

42. A. Mewada, S. Pandey, M. Thakur, D. Jadhav and M. Sharon, *J. Mater. Chem. B*, 2014, **2**, 698–705.

43. S. U. Kumar, I. Matai, P. Dubey, B. Bhushan, A. Sachdev and P. Gopinath, *RSC Adv.*, 2014, **4**, 38263–38272.

44. S. Rello, J. C. Stockert, V. Moreno, A. G'amez, M. Pacheco, A. Juarranz, M. Canete and A. Villanueva, *Apoptosis*, 2005, **10**, 201–208.

45. S. Allen, J. Sotos, M. J. Sylte and C. J. Czuprynski, *Clin. Diagn. Lab. Immunol.*, 2001, **8**, 460–464.

46. S. S. Wang and P. S. Low, *J. Controlled Release*, 1998, **53**, 39–48.

47. Y. H. Lee, F. Y. Cheng, H. W. Chiu, J. C. Tsai, C. Y. Fang, C. W. Chen and Y. J. Wang, *Biomaterials*, 2014, **35**, 4706–4715.

48. P. Chairuangkitti, S. Lawanprasert, S. Roytrakul, S. Aueviriyavit, D. Phummiratch, K. Kulthong, P. Chanvorachote and R. Maniratanachote, *Toxicol. In Vitro*, 2013, **27**, 330–338.

49. C. Riccardi and I. Nicoletti, *Nat. Protoc*. 2006, **1**, 1458−1461.

50. Z. Darzynkiewicz, S. Bruno, B. G. Del, W. Gorczyca, M. A. Hotz, P. Lassota and F. Traganos, *Cytometry,* 1992, **13**, 795−808.

51. A. J. Minn, P. V´elez, S. L. Schendel, H. Liang, S. W. Muchmore, S. W. Fesik, M. C. Fill and B. Thompson, *Nature*, 1997, **385**, 353–357.

52. E. H. Yang, J. Zha, J. Jockel, L. B. Boise, C. B. Thompson and S. J. Korsmeyer, *Cell*, 1995, **80**, 285–291.

53. L. H. Boise, M. Gonzalez-Garcia, C. E. Postema, L. Ding, T. Lindsten, L. A. Turka, X. Mao, G. Nunez and C. B. Thompson, *Cell*, 1993, **74**, 597–608.

54. K. G. Wolter, Y. Hsu, C. L. Smith, A. Nechushtan, X. Xi and R. J. J. Youle, *Cell Biol*., 1997, **139**, 1281–1292.

55. X. Liu, C. N. Kim, J. Yang, R. Jemmerson and X. Wang, *Cell*, 1996, **86**, 147–157.

56. M. O. Hengartner, *Nature*, 2000, **407**, 770–776.

57. S. L. Fink and B. T. Cookson, *Infect. Immun*., 2005, **73**, 1907–1916.
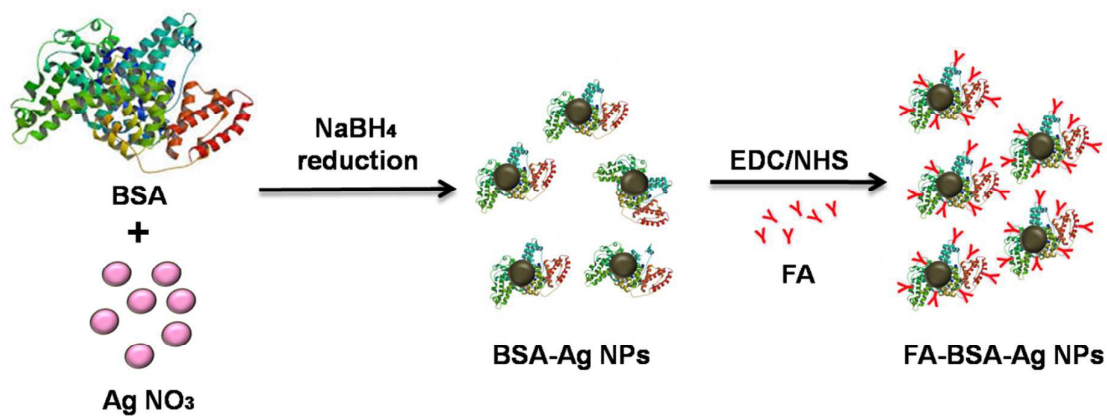
Fig. 1 A schematic representation of preparation of FA conjugated albumin stabilized silver nanoparticles. The structure of BSA (PDB ID: 3V03) was imported from RCSB protein data bank.
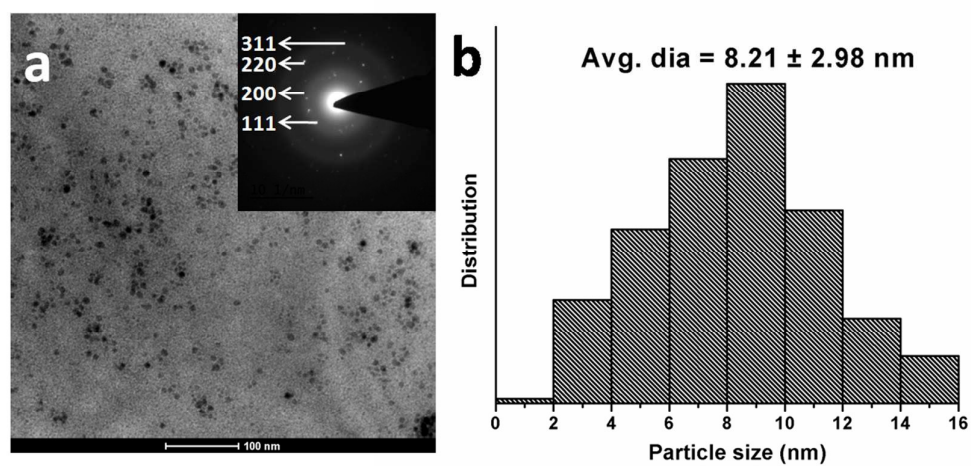
Fig. 2 Characterization of as-prepared FA-BSA-Ag NPs (a) TEM image (scale bar: 100 nm) with corresponding SAED pattern (inset) (b) Particle size distribution histogram of FA-BSA-Ag NPs.
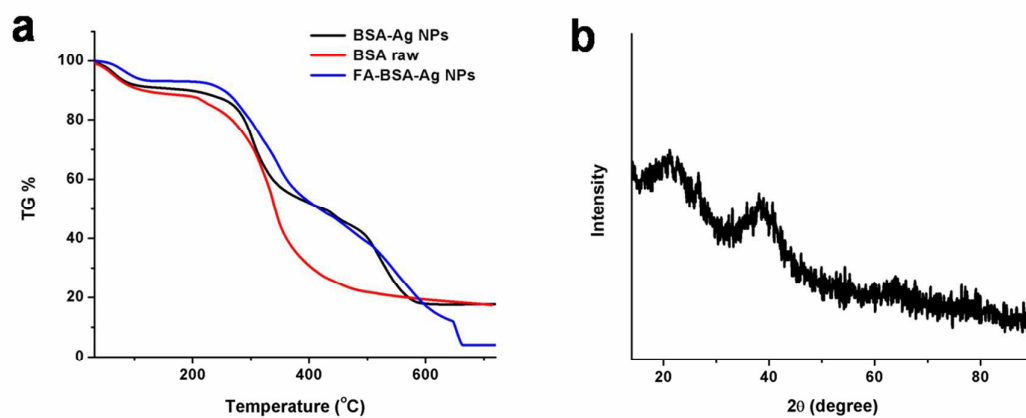
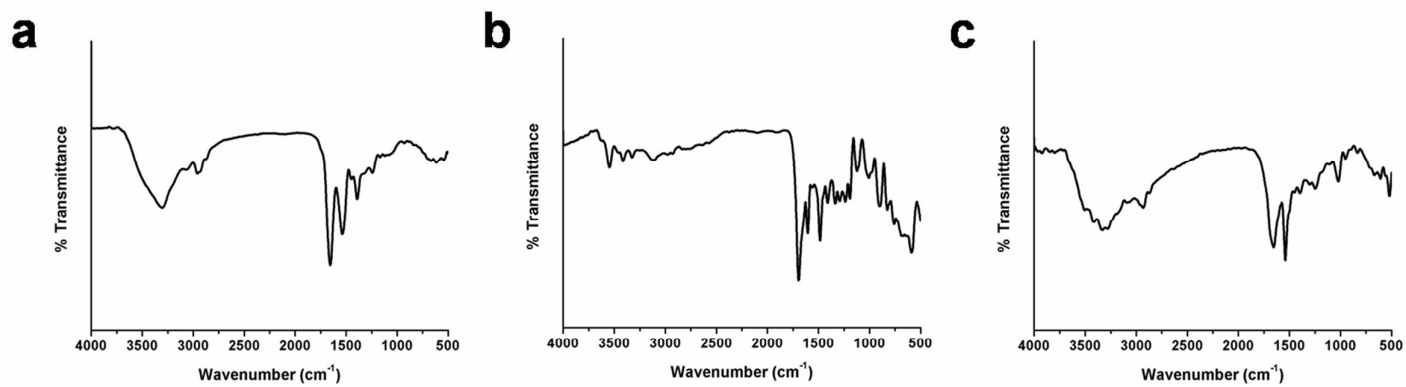**Fig. 3** (a) TG data curve of BSA (control), BSA-Ag NPs and FA conjugated BSA-Ag NPs. (b) XRD pattern of FA-BSA-Ag NPs.

Fig. 4 FTIR spectra of (a) BSA-Ag NPs, (b) FA and (c) FA conjugated BSA-Ag NPs.
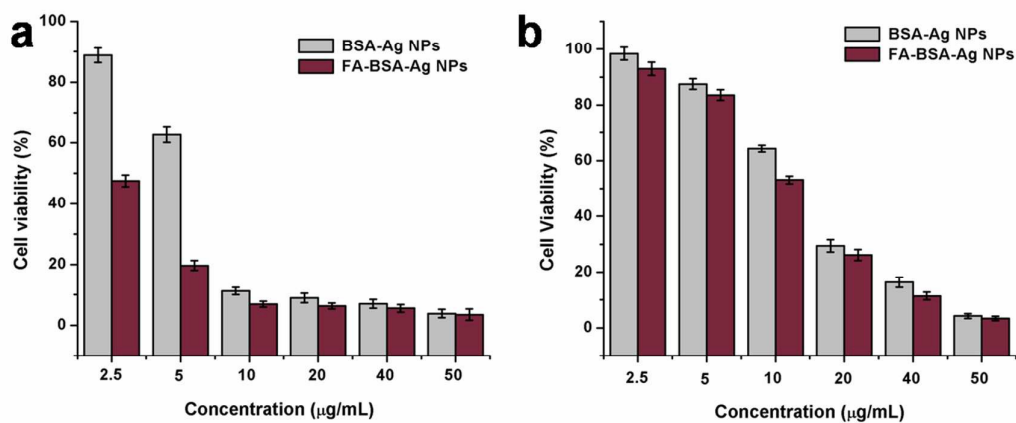
Fig. 5 Cell viability assay (MTT assay) of BSA-Ag NPs and FA conjugated BSA-Ag NPs on

(a) MCF-7 cells (b) A549 cells.
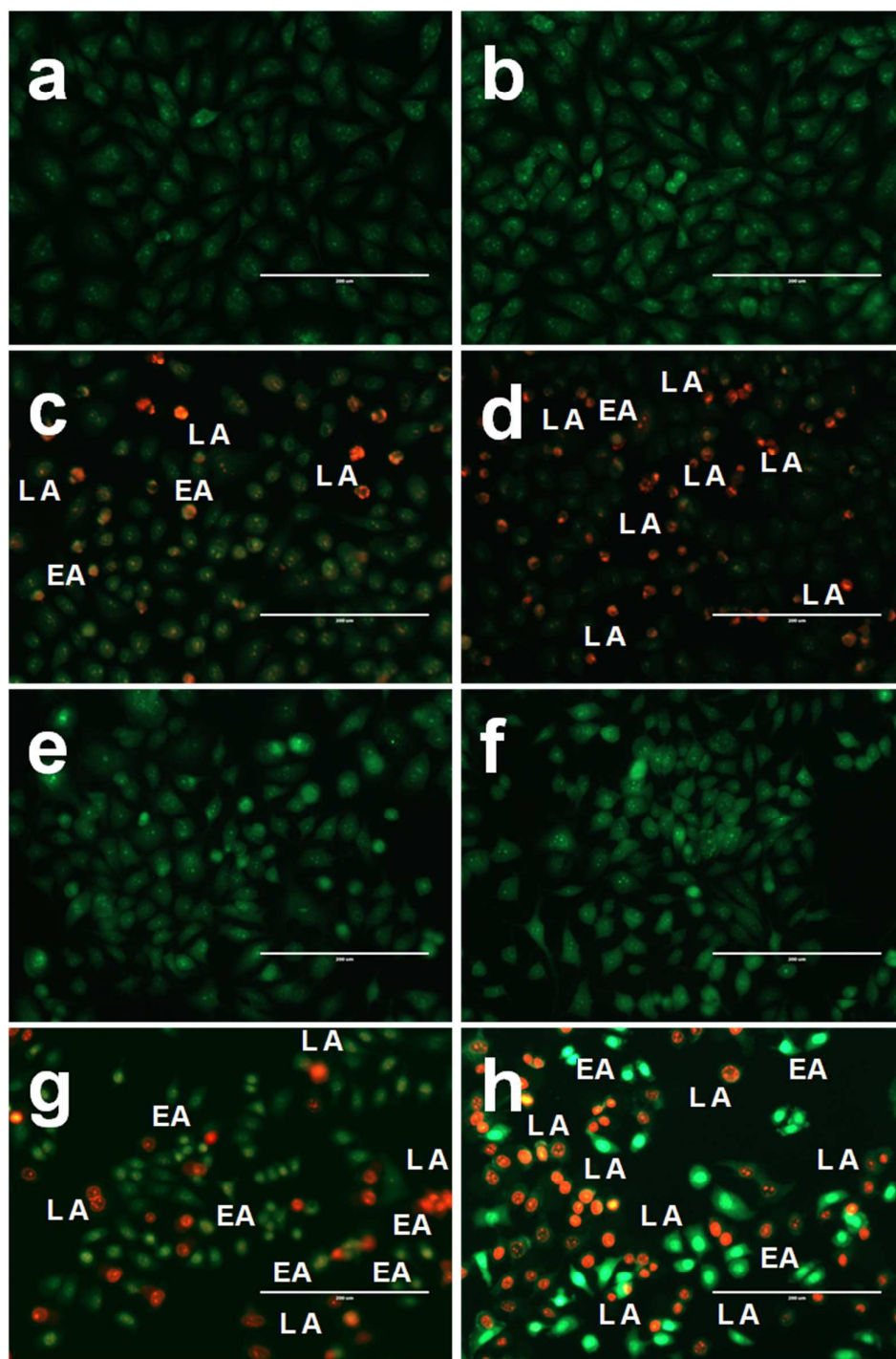
Fig. 6 Representative images of AO/EB dual staining of (a and e) untreated (b and f) 0.5x IC$_{50}$ (c and g) IC$_{50}$ and (d and h) 2x IC$_{50}$ FA- BSA–Ag NPs treated (a-d) A549 and (e-h) MCF-7 cells after 24 h of treatment.
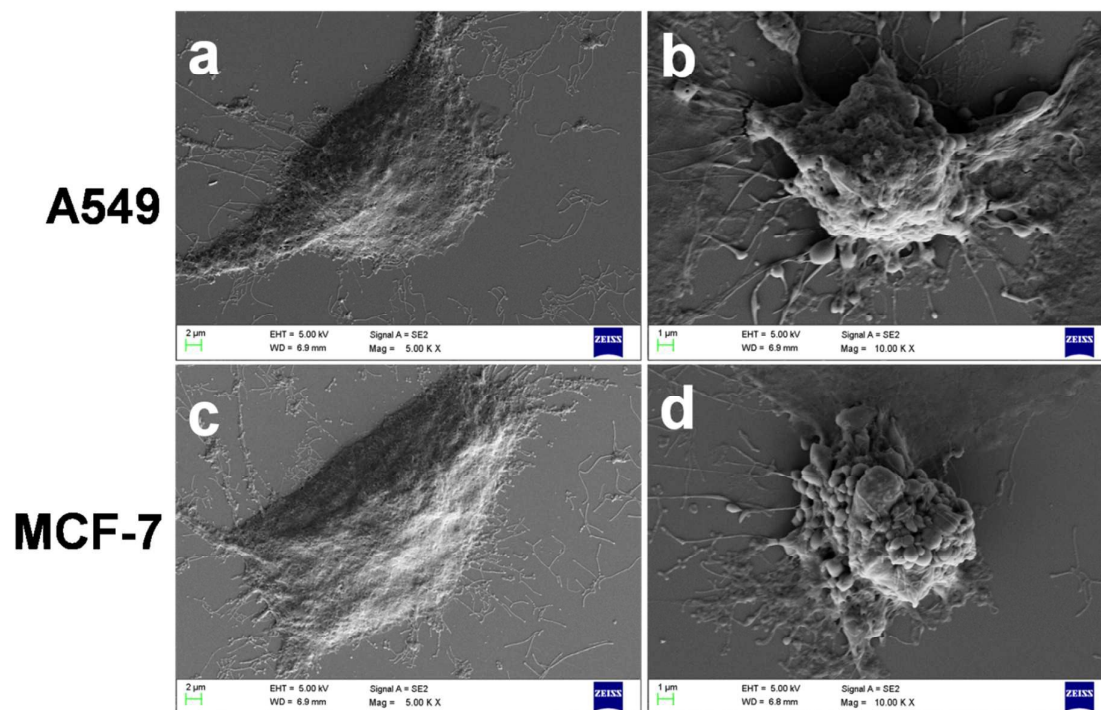
Fig. 7 Representative FE-SEM images of (a and c) untreated and (b and d) treated A549 and MCF-7 cells.
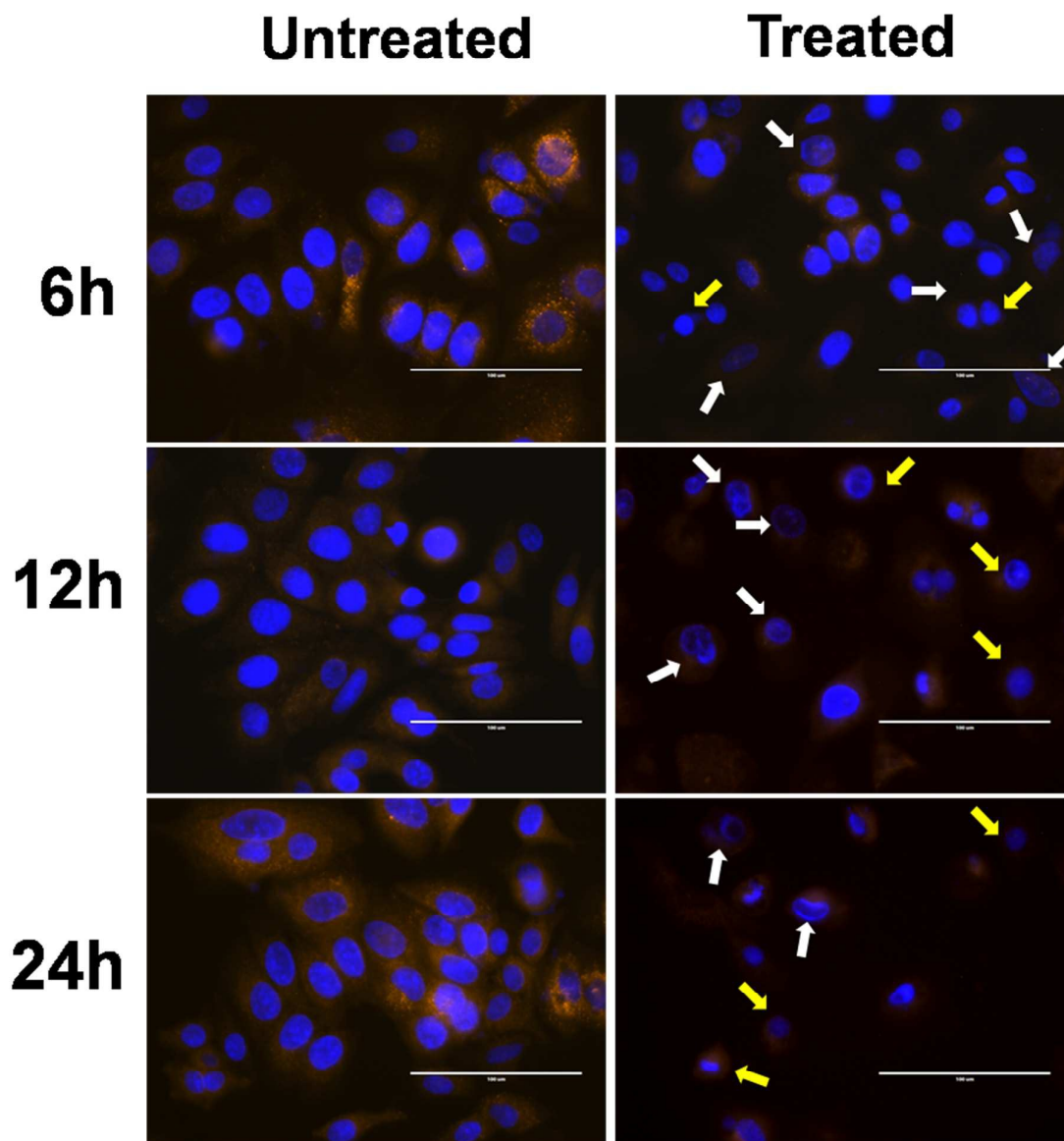
Fig. 8 Time-dependent overlay images of untreated and FA-BSA-Ag NPs (IC$_{50}$) treated MCF-7 cells stained with Hoechst 33342 (blue) and co-stained with rhodamine B (red). White arrows indicate chromatin condensation (dark spots) and yellow arrows point towards cytoskeleton compaction. Scale bar: 100 μm.
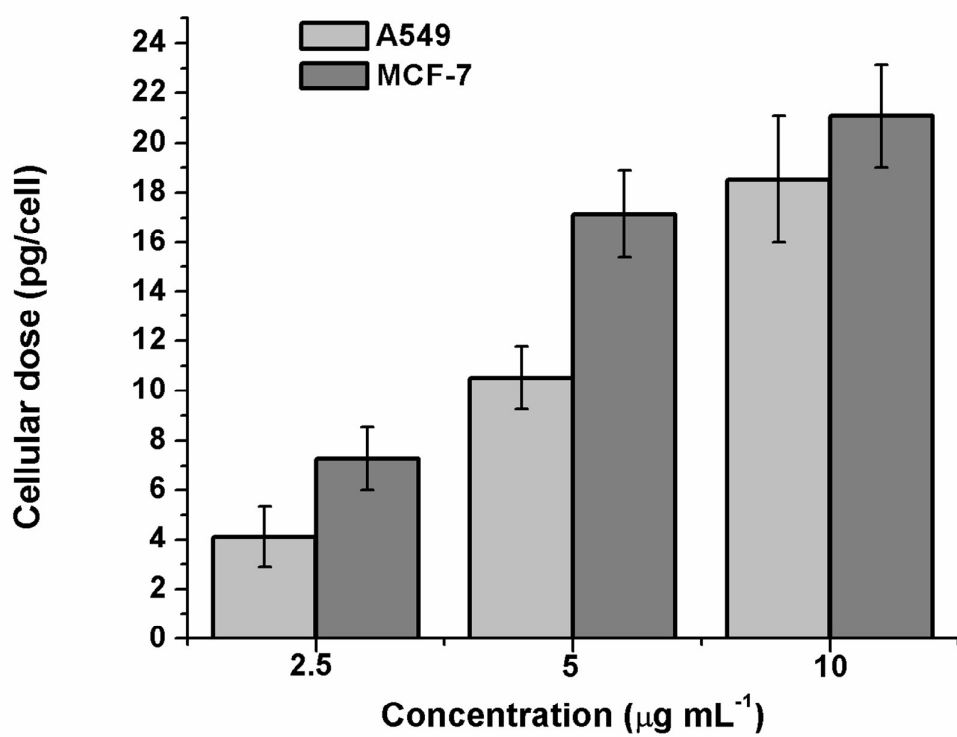
Fig. 9 Cellular uptake of Ag in A549 and MCF-7 cells treated with different concentrations of FA-BSA-Ag NPs after 3 h.
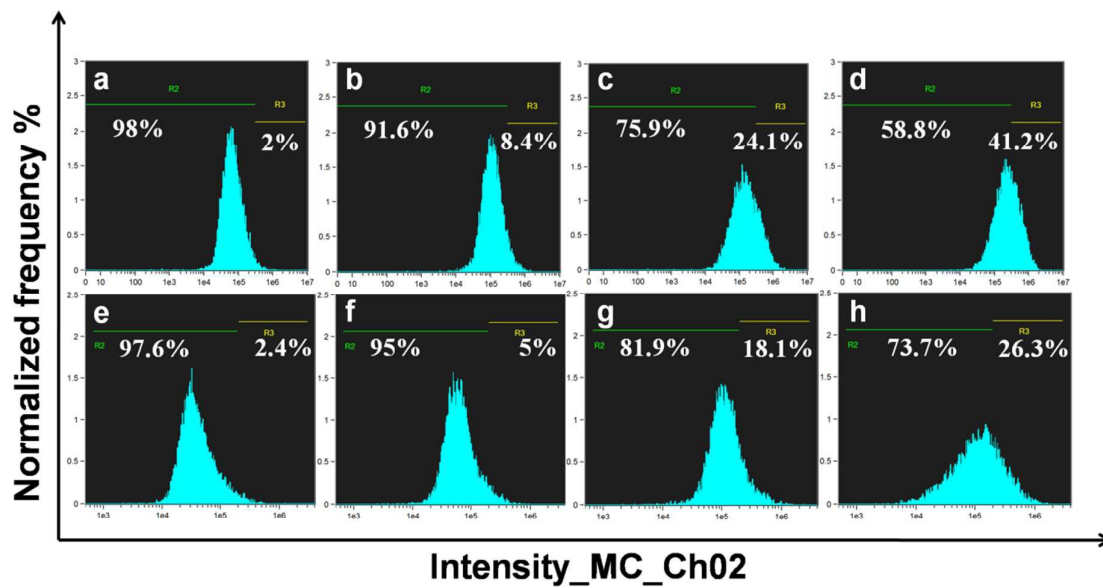
Fig. 10 Flow cytometric analyses of ROS production in A549 and MCF-7 cells treated with different concentrations of FA-BSA-Ag NPs.
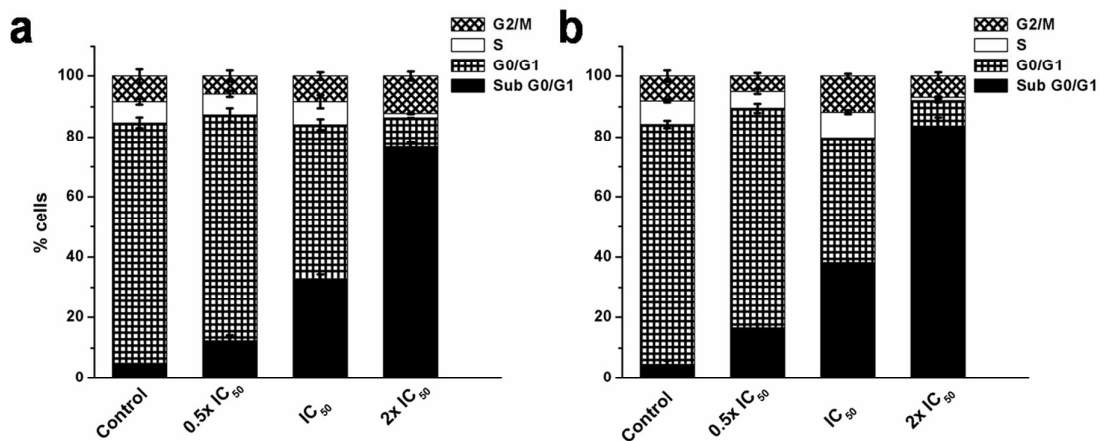
Figure 11 Effect of FA-BSA-Ag NPs on cell cycle in (a) A549 and (b) MCF-7 cells evaluated by calculating the percentage of cells in each phase from flow cytometric data.
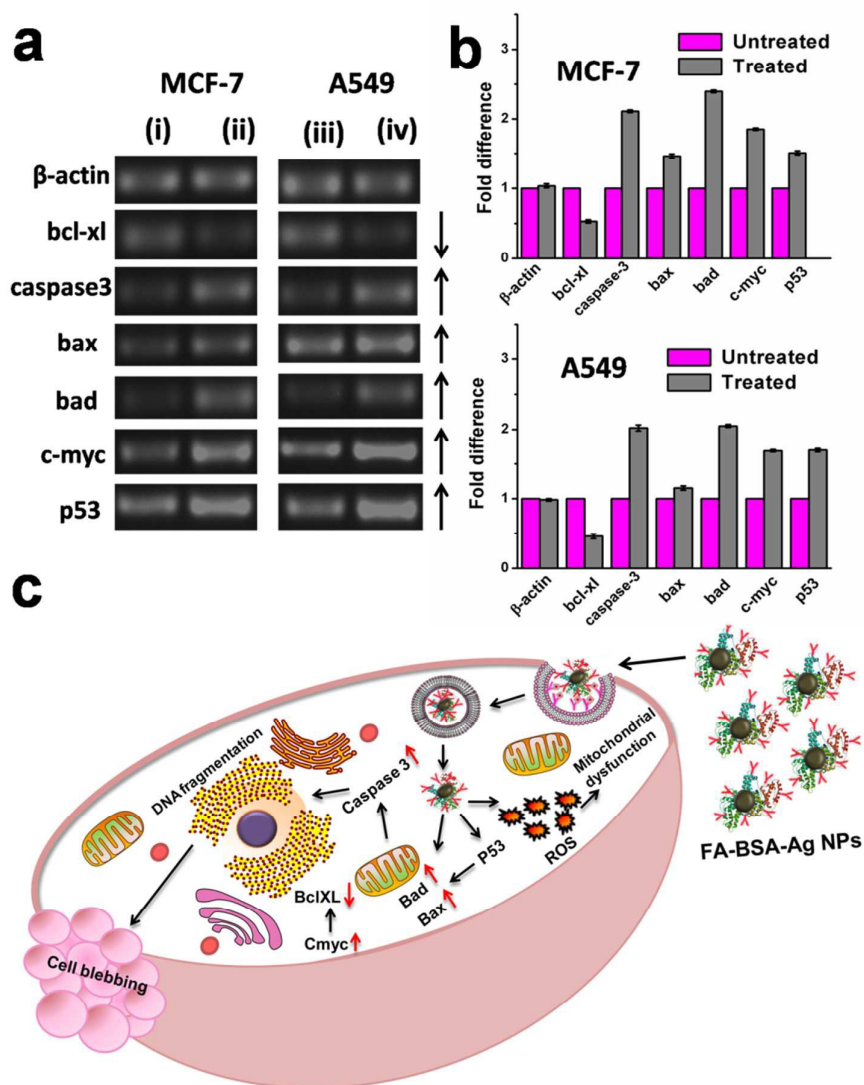
Fig. 12 Semi-quantitative RT-PCR analysis of apoptotic signalling genes (i and iii) untreated control MCF-7 and A549 cells, respectively; (ii and iv) FA- BSA–Ag NPs treated MCF-7 and A549 cells, respectively (b) quantitative expression analysis of apoptotic signalling genes in MCF-7 and A549 cells representing the fold increment in the expression of apoptotic signaling genes in treated cancer cells as compared to the control untreated cells. (c) Schematic representation of FA-BSA–Ag NPs induced apoptosis.